JOURNAL OF BACTERIOLOGY, July 1986, p. 219–230
0021-9193/86/070219-12$02.00/0

Vol. 167, No. 1

Growth Kinetics of Individual *Bacillus subtilis* Cells and Correlation with Nucleoid Extension

I. D. J. BURDETT,[1]* T. B. L. KIRKWOOD,[2] AND J. B. WHALLEY[1]

Laboratories of Cell Surface Interactions[1] and Computing,[2] National Institute for Medical Research, London NW7 1AA, United Kingdom

Received 20 December 1985/Accepted 12 March 1986

The growth rate of individual cells of *Bacillus subtilis* (doubling time, 120 min) has been calculated by using a modification of the Collins-Richmond principle which allows the growth rate of mononucleate, binucleate, and septate cells to be calculated separately. The standard Collins-Richmond equation represents a weighted average of the growth rate calculated from these three major classes. Both approaches strongly suggest that the rate of length extension is exponential. By preparing critical-point-dried cells, in which major features of the cell such as nucleoids and cross-walls can be seen, it has also been possible to examine whether nucleoid extension is coupled to length extension. Growth rates for nucleoid movement are parallel to those of total length extension, except possibly in the case of septate cells. Furthermore, by calculating the growth rate of various portions of the cell surface, it appears likely that the limits of the site of cylindrical envelope assembly lie between the distal tips of the nucleoid; the old poles show zero growth rate. Coupling of nucleoid extension with increase of cell length is envisaged as occurring through an exponentially increasing number of DNA-surface attachment sites occupying most of the available surface.

For 20 years the replicon hypothesis (22) has continued to provide a framework for understanding bacterial growth and division. The central feature of the hypothesis is that the replicated daughter chromosomes, attached to the membrane, would be segregated by zonal insertion of newly synthesized membrane between the points of attachment. Coordination of growth and division would therefore be mediated by the membrane, with the position of the chromosome occupying a critical role in determining the site of growth (22, 27, 34, 43, 47, 48).

Zonal growth of the wall has been clearly demonstrated in streptococci, where raised wall bands mark the junction between old and new wall (19). In bacilli the position is less clear, and evidence for both zonal (7, 21) and diffuse (11, 35) growth has been reported. Although wall bands marking the limit of septal and cylindrical wall have been reported in *Bacillus subtilis* (4), there are no known external markers for delimiting the cylindrical growth site. A recurrent problem in the study of bacilli is therefore the difficulty of determining the number and extent of sites of cylindrical envelope assembly.

Autoradiographic studies with light microscopy have suggested the existence of large "segregation units" in the walls of *B. subtilis* (50, 51). The number of these units apparently increases with the richness of the medium, although the resolution of the technique did not permit the number of segregation units generated per growth zone or the location and size of each zone to be determined. However, others (27) have interpreted the data to mean only that completed poles are conserved, not that there is zonal insertion of new wall. Present conceptions of wall assembly in bacilli suggest that the surface enlarges by a process of inside-to-outside growth, thus conferring some degree of mobility upon nascent wall constituents (1, 24, 41, 42). Lateral movement (spreading) of newly synthesized wall also probably occurs, so that the point of insertion does not match the site where the layer of wall ultimately reaches the surface (41, 42). Such a process would clearly constrain attempts to label the surface and observe a segregation pattern.

The mechanisms of surface extension also have consequences which bear directly upon the kinetics of growth of the individual cell. For example, if growth were linear and new wall was inserted at a particular time in the cycle, an abrupt increase in the rate of length extension would be observed, corresponding to a duplication of growth zones. Several formal models for envelope assembly, invoking bilinear or exponential kinetics for length extension or surface area expansion, have been described (26, 28, 32, 36, 38, 40, 44, 47, 48). Although growth between divisions is thought to be continuous, it is not known how the rate of extension may change with time. We have reviewed some of the approaches used to determine the growth kinetics of individual cells (5) and concluded that methods like that of Collins and Richmond (8), which calculate the rate of growth as a function of cell size, afford the most powerful method of distinguishing one growth pattern from another. Our modification of this approach also allows the growth rate to be calculated for mononucleate, binucleate, and septate cells (5).

In the present study we have addressed three aspects of bacterial growth and division. (i) Does the rate of length extension vary in the cell cycle, (ii) can the rate of growth of the nucleoid be correlated with the growth rate of the cell, and (iii) can the limits of the cylindrical growth zone be determined?

MATERIALS AND METHODS

Bacterial strain and growth conditions. *B. subtilis* 168/S (4, 46, 47), which is able to grow on succinate as a sole carbon source, was grown at 35°C in minimal medium (47) with 0.5% glucose for six generations and then transferred to medium containing 0.4% sodium succinate. Cultures were inoculated from a single colony and periodically subcultured over 3 days to maintain an absorbancy at 600 nm of <0.3.

Electron microscopy. (i) Fixation and embedding. Samples (5 to 10 ml) were prefixed with formaldehyde-glutaraldehyde

* Corresponding author.

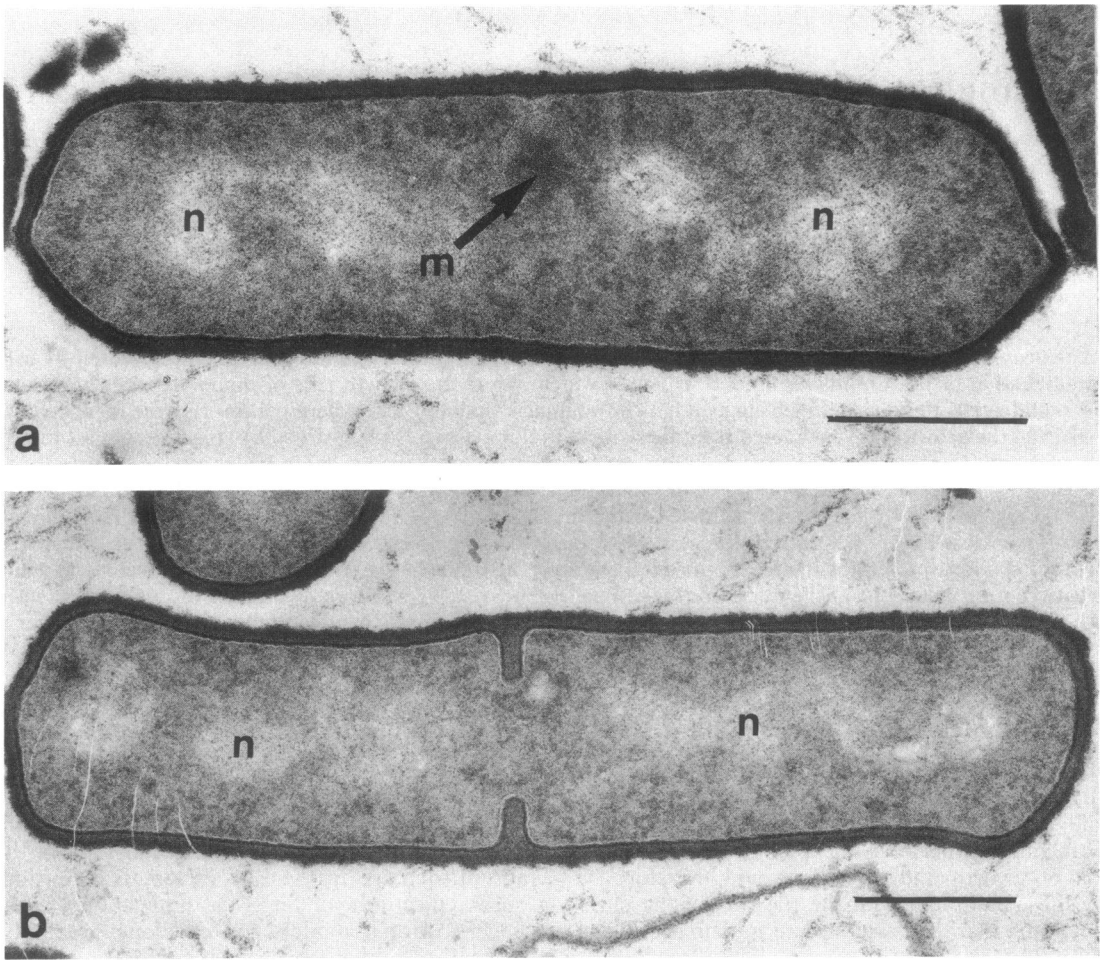

FIG. 1. Electron micrographs of longitudinal thin sections of *B. subtilis*. (a) Early binucleate cell with divided nucleoid (n) and central mesosome (m); this cell corresponds to stage 3 or binucleate 1 in Fig. 3. (b) Initiation of cross wall with separated nucleoids (n); note the slightly increased diameter near the cross wall and at distal poles. Bars, 0.5 μm.

or with OsO_4 as previously described (3, 4). After enrobing with 2% agar, pellets (<1 mm^3) were postfixed overnight in 1% OsO_4 (23), washed for 2 h in 0.5% uranyl acetate (23), dehydrated in ethanol, and embedded in Epon. Sections were cut with a diamond knife and picked up onto copper-rhodium grids covered with a carbon film. Sections were stained with uranyl acetate and lead citrate.

(ii) CPD. Samples (5 to 10 ml) were prefixed with 0.1% OsO_4 (23) for 10 min and then suspended in 1% OsO_4 for 60 min at room temperature. After samples were washed in sterile distilled water by centrifugation, droplets (about 50 μl) were deposited for 30 min onto grids covered with a carbon-Formvar film held between clamped forceps. The grids were previously floated, face down, for 5 min onto drops of 1% Alcian blue on sheets of dental wax and then washed in two changes of distilled water to provide a positively charged surface (39). The grids were used within 30 min of preparation. Individual grids were then mounted in distilled water in a grid holder supplied with a Polaron critical-point-drying (CPD) unit (Polaron Equipment, Watford, United Kingdom) and then dehydrated in ethanol by the following regime: 50% (1 h), 70% (1 h), 90% (1 h), and absolute ethanol three times (overnight). After the last ethanol wash, the grid holder was placed in the CPD unit and flushed three times with liquid CO_2 over a 1-h period (58).

(iii) Agar filtration. Parallel samples (1 to 2 ml) were also prefixed with 0.3% paraformaldehyde–0.1% glutaraldehyde and prepared for agar filtration (2, 58). Prefixation with aldehyde, rather than OsO_4, was found to be necessary to avoid distortion and plasmolysis of cells upon air drying.

All specimens were examined in a JEOL 100 CX electron microscope at 60 kV; the microscope was fitted with a high-resolution tilting stage. CPD-prepared samples were initially examined with minimum illumination to avoid speciment distortion. The magnification was calibrated with the replica of a diffraction grating (2,160 lines per mm; Agar Aids, Bishop's Stortford, United Kingdom).

Measurements of cell size. Linear measurements of profiles of cells prepared by CPD or agar filtration were traced onto a graphics tablet interfaced to a PDP 11 minicomputer or to an Apple II microcomputer. The methods, assumptions, and accuracy of the technique have been described previously (3, 4).

Statistical analysis. Basic statistics concerning the size distributions of cell profiles obtained by electron microscopy were calculated with a DEC 2060 computer. Additional analyses were obtained with an Apple II microcomputer.

Comparisons of size distributions were made by using the two-sample Kolmogorov-Smirnov nonparametric test (52). This test contrasts the maximum difference (D_{max}) in cumu-

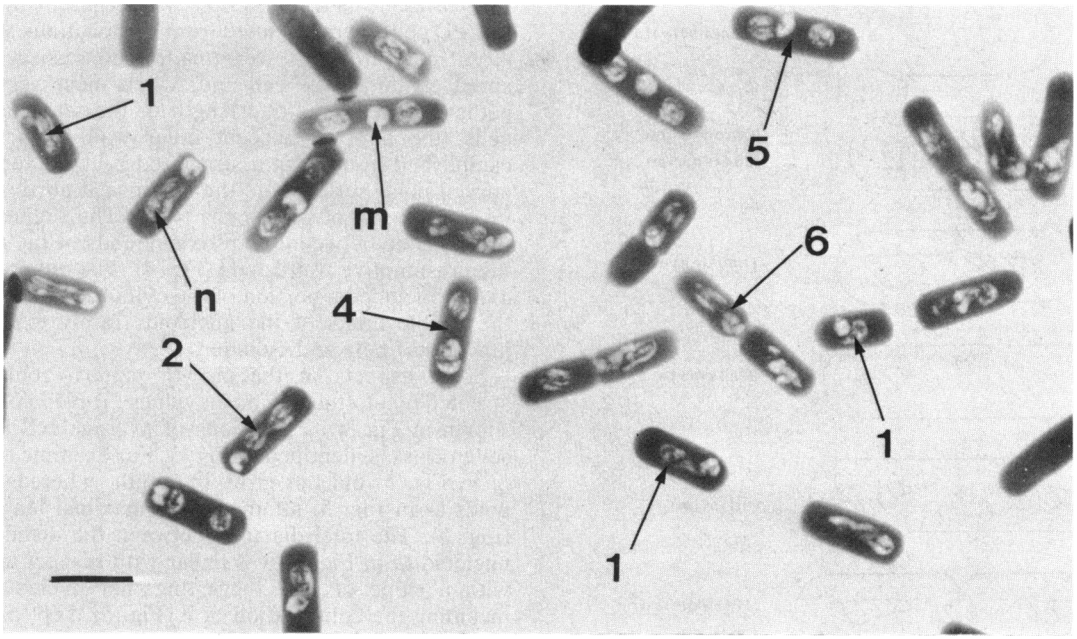

FIG. 2. Electron micrograph of a portion of a field of CPD cells of *B. subtilis*. Nucleoid (n) is visible as a vacuole containing coagulated fibrils; a mesosome (m) is an empty vacuole. Numbers point to cells corresponding to stages identified in Fig. 3, but not all stages are present in this field. Bar, 1 μm.

lative frequency between the two distributions with critical values (D_{crit}) tabled according to sample size. If D_{max} is less than D_{crit}, the difference between the distributions is not statistically significant at the chosen level of the test (usually $\alpha = 0.05$).

The method of growth rate calculation was an extension of the method of Collins and Richmond (8; T. B. L. Kirkwood and I. D. J. Burdett, manuscript in preparation). See Appendix for growth rate calculations.

RESULTS

Verification of steady-state growth. Our method of analysis, like that of Collins and Richmond (8), depends upon obtaining a stable length distribution. Tests for deviation from steady-state growth were made by comparison of length distributions by using the nonparametric Kolmogorov-Smirnov test (52) with a probability level of $\alpha = 0.05$. Three samples for electron microscopy were taken on day 3 of growth at 35°C; the second and third samples were harvested 55 and 85 min after the first sample. Because cells might be lost during the mounting procedure for CPD, thus yielding an unrepresentative sample, analyses of length distribution were also made with agar-filtered samples not subjected to centrifugation or washing. Comparison of the cumulative frequencies of the three samples, comprising 779, 631, and 746 cells, respectively, showed that in no case was the maximum deviation ($D_{max} = 0.037$ to 0.050) between samples greater than the calculated critical difference ($D_{crit} = 0.0697$ to 0.0736) at $\alpha = 0.05$.

CPD samples were also compared in this way. Values for D_{max} (0.032 to 0.0555) again did not exceed D_{crit} (0.06705 to 0.075) at $\alpha = 0.05$. A total of 2,097 CPD cells were measured, composed of 863, 546, and 688 cells for each sample. Tilting the specimens over angles of ±10 to 40° showed that the majority of cells were apparently lying flat upon the grid.

Application of the Kolmogorov-Smirnov test therefore showed that there were no significant differences in the measured distributions over time, and histograms of the different samples showed that they were sufficiently similar to be regarded as a single distribution. However, the average length ± the standard deviation of CPD cells (1.38 ± 0.36 μm) was approximately 25% shorter than that of air-dried, agar-filtered cells (1.84 ± 0.46 μm), as reported for *Escherichia coli* (58). The cumulative frequencies of CPD and agar-filtered cells were therefore compared, after normalization, by using the Kolmogorov-Smirnov test at $\alpha = 0.05$; D_{max} (0.036) was less than D_{crit} (0.0411). Therefore, although reduced in length, the shape of the distribution of cell length in CPD samples was comparable to that of air-dried cells. The implications of this finding are that the size distribution obtained from CPD preparations contains all representative classes of cells and that the amount of shrinkage is the same for all cells.

The doubling time (T_D) of the culture, as measured by the increase in absorbancy at 600 nm, was 120.08 ± 2.16 min (mean ± standard deviation). The specific growth rate (k) was 0.0058 ± 0.0001 doubling times per min.

Morphology of sectioned cells. A simulated sequence of events comprising the division cycle was first reconstructed from 276 median, longitudinal sections of cells prefixed with aldehydes and OsO_4. Among the smaller, nonseptate cells the nucleoid appeared as a centrally located bundle of fine fibrils. Occasionally the nucleoid was associated with a polar mesosome. Nucleoid morphology altered to a pronounced dumbbell shape in larger cells. Where two lobes of the nucleoid were present, but no cross wall, a centrally located mesosome was often observed (Fig. 1a).

Septum formation was essentially similar to that described for strain 168/S grown in glucose minimal medium (4), where septal closure was preceded by cross-wall separation. Stages of cross wall initiation were often marked by slight reductions in diameter along the cylindrical portion of the cell (Fig. 1B) in sections judged by criteria as diagnostic of median sections (4, 19), i.e., a fully tribanded wall. The base

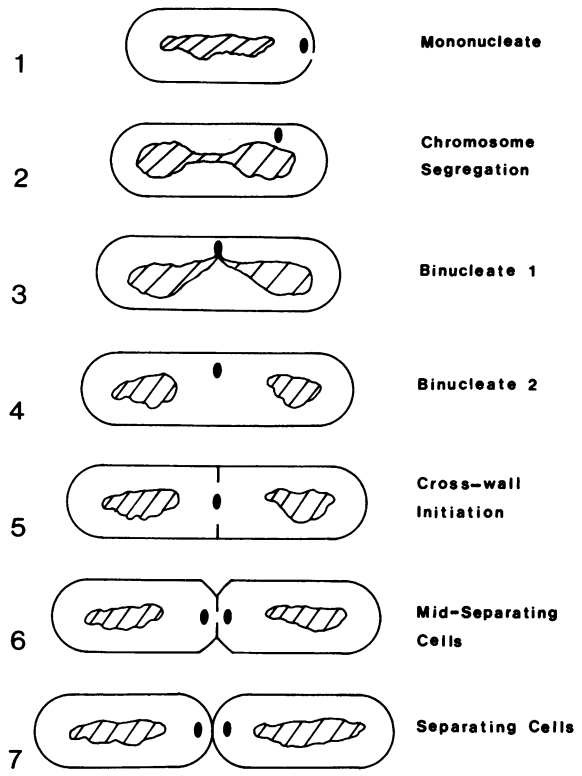

FIG. 3. Diagram showing main categories of cells identified in CPD preparations. The nucleoid is shown as cross-hatched, and the mesosome is shown as an opaque dot; the shapes of the cells are purely diagrammatic.

of the cross wall and the distal poles therefore appeared of slightly greater diameter than the cylinder (Fig. 1b). A very similar sequence was found in material fixed solely by OsO_4.

Morphology of CPD cells. The object of preparing specimens by CPD was to obtain cells transparent to electrons, where the principal stages of the cycle, as described above, could be scored and measured in substantial numbers (Fig. 2). Organisms fixed with aldehydes and a small proportion of OsO_4-fixed cells prepared by CPD were relatively opaque to electrons. In well-spread preparations fixed with 1% OsO_4, stages of the cycle identified in sectioned organisms were seen and classified into seven distinct categories (Fig. 3). The micrographs were scored independently by two of us; the few discrepant cells which arose were resolved by consensus. The most difficult stages to identify were binucleate, nonseptate cells (Fig. 3) and some cells initiating a cross wall. Many of the cells placed in the latter category showed the same variation in diameter as seen in sectioned cells (Fig. 1B).

Coagulated strands were seen in the nucleoids, in contrast to the fine strands observed in sectioned organisms. However, the profiles of nucleoids seen in CPD cells were comparable to those seen in sections. Mesosomes (Fig. 2) were present as small vacuoles. Although currently regarded as organelles of doubtful status, their location appeared to vary in a systematic way, as described by Highton (20). A centrally located mesosome was observed in association with a nearly separated nucleoid, i.e., binucleate 1 cells (Fig. 3). Thereafter, mesosomes appeared to be confined to the developing cross wall (Fig. 3) or to one pole of mononucleate cells (Fig. 3).

Measurements from CPD cells. Measurements of features in CPD cells were obtained from the locations shown in Fig. 4. All measurements were made with respect to the measured center of the cell and, where necessary, added together to yield the total length of the feature. In dividing cells, the limit of nascent polar wall (*e* in Fig. 4) was established by placing a straightedge at the junction of the curved polar surface and the cylindrical portion of the cell, i.e., at the site of wall bands (4, 6). The segment *c* marked the distance between the proximal ends of the nucleoid and the presumptive wall bands (Fig. 4). The old poles (*g* in Fig. 4) also included a portion of the cylindrical surface, because the visible limits of the nucleoids rarely extended to the junction of pole and cylinder.

Some aspects of the growth pattern could be reconstructed by plotting the mean values (Table 1) of the features shown in Fig. 4 as functions of average cell length of the seven classes identified in Fig. 3. For example, the old poles (*g* in Fig. 5) did not grow in length, whereas the nascent poles (*e* in Fig. 5) attained their maximal length gradually (Fig. 5). The total distance between the distal ends of the nucleoid (*a* in Fig. 5) was linear with respect to cell length, with a slope of 1.0, suggesting that nucleoid extension, including the contribution of *c* (Fig. 5), kept pace with cell elongation. Subtraction of the size of nascent poles (i.e., *a* −

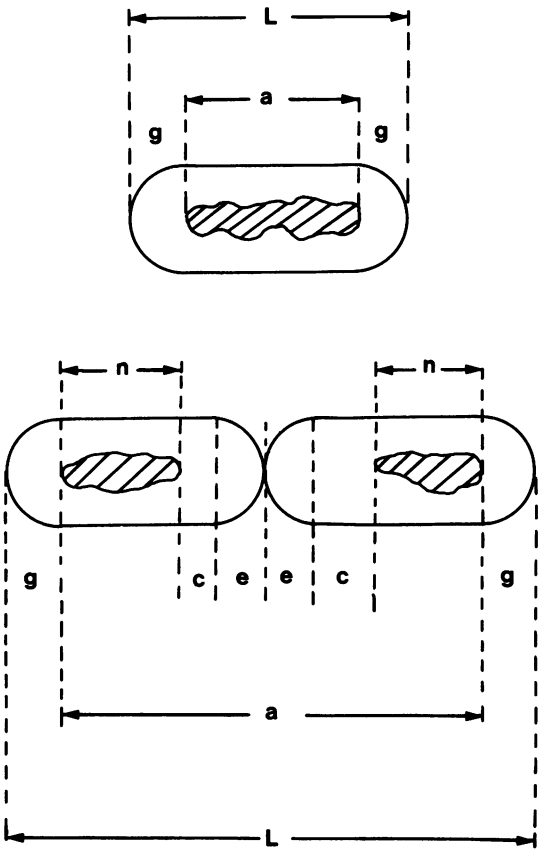

FIG. 4. Diagram showing locations where measurements were taken of CPD cells. *L*, Total length of cell; *a*, distance between distal tips of nucleoids; *n*, length of individual nucleoids; *g*, length of distal (old) poles; *e*, length of nascent poles; *c*, distance between limit of nucleoid and junction with nascent polar wall. For nonseptate cells (upper diagram), *a* is the total length of nucleoid and *c* and *e* are absent.

TABLE 1. Mean values for cell length and nucleoid lengths in *B. subtilis*, measured from CPD preparations[a]

Category	No. of cells	$\bar{L}$ ± SD (CV)	$\bar{N}$ ± SD (CV)
Mononucleate	536	0.98 ± 0.19 (0.19)	0.51 ± 0.14 (0.27)
Chromosome segregation	243	1.21 ± 0.16 (0.13)	0.73 ± 0.14 (0.19)
Binucleate 1	327	1.24 ± 0.18 (0.15)	0.76 ± 0.16 (0.21)
Binucleate 2	245	1.36 ± 0.18 (0.13)	0.89 ± 0.13 (0.14)
Cross-wall initiation	340	1.55 ± 0.27 (0.18)	1.05 ± 0.24 (0.23)
Midseparating	331	1.73 ± 0.29 (0.17)	1.13 ± 0.26 (0.23)
Cross-wall separation	75	1.97 ± 0.34 (0.17)	1.20 ± 0.34 (0.28)

[a] $\bar{L}$, Average cell length; $\bar{N}$, average distance between distal ends of nucleoids, i.e., ($a - 2e$; Fig. 4); CV, coefficient of variation.

$2e$) showed that the relationship became nonlinear as septation progressed. The fraction of cylindrical wall (c in Fig. 5) lying adjacent to the nascent poles also appeared to increase in length, although the slope of the line was not as steep as that relating nucleoid length (n in Fig. 5) to mean cell length. The mean lengths of individual nucleoids (n in Fig. 5) after segregation were actually slightly smaller than expected by assuming equal division of the nucleoid into two halves. This suggests that, on separation, the daughter nucleoids round up slightly (elastic recoil?) and then gradually enlarge (Fig. 5).

Rate of length extension. The essentially geometric relationships shown in Fig. 5 did not provide a measurement of the rate of growth or reveal the underlying pattern. The calculated rate of length extension plotted as a function of cell length is shown in Fig. 6 for mononucleate, binucleate, and septate cells, from equations described in the Appendix. The inset to Fig. 6 emphasizes the differences obtained when the rate of growth (linear, bilinear, or exponential) was plotted as a function of cell size in the ideal or canonical form (25). The shapes of the curves relating the calculated rate of length extension to cell length were neither linear nor bilinear, but most closely resembled an exponential mode of increase (Fig. 6). Although the rate of extension increased with cell length, there was also overlap between the size classes, e.g., the larger mononucleate cells extended into the lower size range of binucleate cells. Also shown in Fig. 6 is the rate calculation with the Collins-Richmond (8) equation, based on the frequency distribution of newborn, dividing, and extant cells, which coincided with the rates of extension for smaller mononucleate and larger septate cells. The remaining portion of the Collins-Richmond curve, representing the bulk of the population, was also nearer to an exponential rate of increase and represented an averaging of the growth rate obtained when mononucleate, binucleate, and septate classes were considered separately (Fig. 6). The old poles (g in Fig. 4) showed zero growth rate (data not shown).

The rates of length extension showed no evidence of a bilinear increase, although such a growth pattern has been proposed for both *B. subtilis* and *E. coli* (43, 44, 47). We therefore examined whether it was possible to obtain bilinear growth by modifying the distribution of cell size, in particular those of cells undergoing chromosome segregation or cross-wall initiation. If a bilinear growth pattern was present and was correlated with a doubling in the number of zones of envelope assembly, it is at these points that the postulated time of duplication is most likely to occur. Since these points were also the hardest to score precisely from the electron micrographs, the possibility was considered whether the distributions of cell lengths for these two categories of cells were too broad (see Appendix). Accordingly, the standard deviations of the length distributions of cells in these two

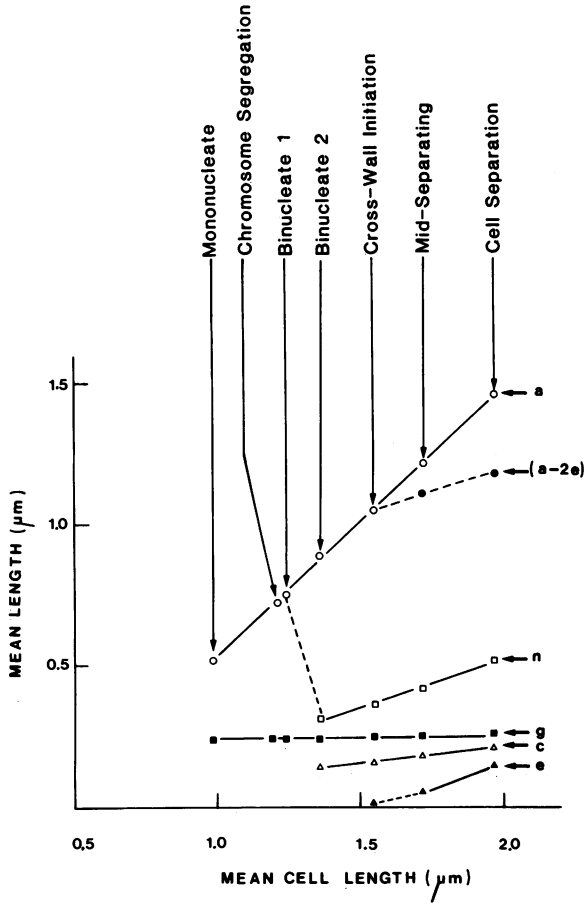

FIG. 5. Relationship between average values (ordinate) of measured variables (a, n, g, c, e; see Fig. 4) and mean cell length (abscissa) corresponding to classes of cells shown in Fig. 3. Note that total distance, a, between nucleoids has a slope of 1.0, whereas there is a decline in this relationship when the contribution of nascent poles is omitted, i.e., $a - 2e$. At nucleoid segregation (dashed line connecting a to n), there is slight reduction in average nucleoid size which is only restored to mononucleate size at cell separation. The old, distal poles (g) show no increase in size with increase of average cell length, i.e., the slope is not significantly different from zero. Cylindrical walls (c) between nucleoids and nascent poles continue to increase in size after the binucleate 2 stage; nascent poles (e) are produced at the midseparating stage (stage 6 in Fig. 3).

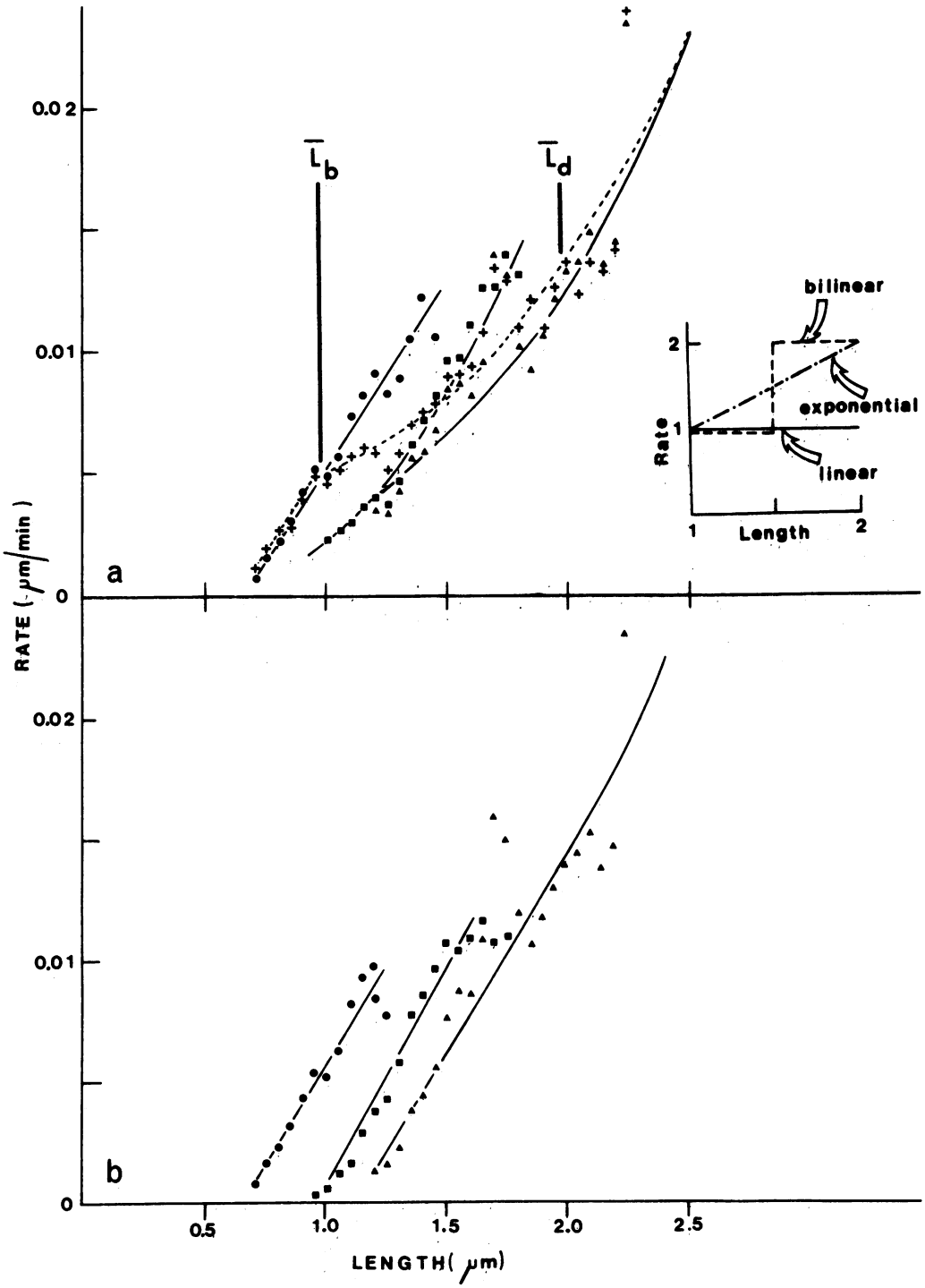

FIG. 6. Rate of growth of cell length as a function of cell length for mononucleate, binucleate, and septate cells. (a) Standard deviations without reduction, showing mononucleate (●), binucleate (■), and septate (▲) cell lengths. Also shown is the growth rate for length (+) calculated according to the Collins-Richmond equation (8), which closely follows the lower region of mononucleate cells and the upper region of septate cells. The inset emphasizes the differences between exponential, bilinear, and linear rates of extension as functions of cell length in an idealized case. (b) Standard deviations of chromosome-segregating and cross-wall-initiating cells, both reduced ×0.75. Symbols as in a. Note close similarity to graph shown in a. The data were not subjected to smoothing, and the upper and lower 2.5% of the distributions were omitted because calculations near the tails of the frequency distribution are subject to large statistical variation. The mean lengths of newborn ($\bar{L}_b$) and separating ($\bar{L}_d$) cells are indicated.

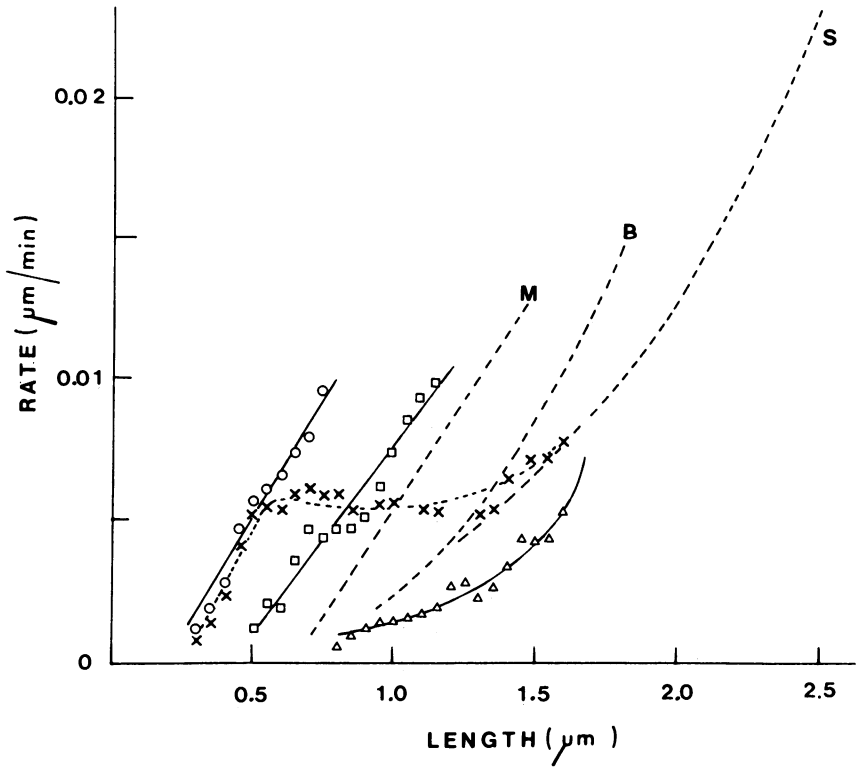

FIG. 7. Rate of growth of nucleoid distance ($a - 2e$ [Fig. 4]) as a function of cell length for mononucleate (○), binucleate (□), and septate (△) cells. Also shown is the rate of nucleoid extension (×) calculated by means of the Collins-Richmond equation (8). The dashed lines represent curves taken from Fig. 6a to emphasize that the rates of length extension of mononucleate (M), binucleate (B), and septate (S) cells are essentially parallel to the rates of nucleoid extension.

categories were reduced by a factor that varied from 0.9 to 0.75, while keeping the means constant. No major change in the growth pattern was observed (Fig. 6).

Rate of nucleoid extension. Shown in Fig. 7 are results for the rate of nucleoid extension plotted as a function of nucleoid length (i.e., $a - 2e$ in Fig. 4). For mononucleate and binucleate classes the slopes of the rates of cell length extension were approximately parallel to those of nucleoid extension (Fig. 7). The rates for nucleoid extension were approximately exponential and showed no evidence of a linear or bilinear pattern. No straightforward statistical comparison could be made, because the values do not represent independent observations. Only among the septate cells was there any obvious nonparallelism (Fig. 7). Also shown in Fig. 7 is the rate of nucleoid extension calculated by means of the Collins-Richmond equation (8). Adjustment of the standard deviation by the method described above did not lead to any major change in growth rate (data not shown).

DISCUSSION

Duration of cell cycle events. The numbers of cells in each of the three classes, mononucleate, binucleate, and septate (Table 1), can be used to calculate the approximate timing of some events in the cell cycle by means of the theoretical age distribution (9). Thus, nucleoid segregation occurs at about 70 min (0.59 generation) before cell separation, whereas septation is initiated at about 58 min (0.48 generation) before septation. Splitting of the cross wall occupies about 36 min (0.3 generation). Values for the total septation time derived from agar-filtered cells gave a value of 32 min, suggesting that the CPD preparations do not yield unrealistic estimates.

The data do not, of course, yield estimates of the time required (C period; 10) for chromosome replication. C values of 45 min (36) and 53 min (14) have been reported, but the C period may be greatly extended in thymine-requiring strains of *B. subtilis* cultured at low growth rates (14). From shift-up experiments with strain 168/S, the C period may be about 180 min in succinate-grown cultures (46). Chromosome replication therefore extends over two cycles. The morphological criteria used to classify cells as mononucleate or binucleate are made without reference to genome content. Thus, at birth, a cell contains a partially replicated chromosome. Segregation of the nucleoid in midcycle (Fig. 3 and 6) has also been reported by Sargent (47), although the appearance of nucleoids in OsO_4- or aldehyde-fixed cells differs markedly from that of those in heat-fixed, Giemsa-stained preparations (47). Recent studies of the shape of the nucleoid in *E. coli* B/rH266 (T_D, 21 min) have shown that very similar images can be obtained from OsO_4- or glutaraldehyde-OsO_4-fixed material when compared with living cells visualized by confocal scanning light microscopy (54).

In addition, we have visualized nucleoids in living cells of *B. subtilis* exposed to the DNA-specific dye DAPI (unpublished observations); the nucleoids are very similar in shape to those reported here in CPD preparations. Hariharan et al. (17) have also shown that nucleoids of a temperature-sensitive DNA initiation mutant adopt a doublet shape after one or two rounds of replication are allowed to go to completion. They emphasize that their observations are

consistent with a gradual pulling apart of a single mass of DNA into two lobes. Although these observations, and our own, are not consistent with the abrupt separation of nucleoids seen in heat-fixed cells (47), all reports agree that ultimately the daughter nucleoids do come to occupy definite sites in the cell.

Kinetics of growth. The results shown in Fig. 6 show no evidence of linear or bilinear rates of length extension but are more consistent with an exponential pattern of increase. Among the larger binucleate and septate cells, however, there appears to be a significant deviation from a strictly exponential curve proportional to cell size. This type of "accelerated" exponential growth in length has also been reported by Errington et al. (15) and in *Bacillus cereus* (8) as well as several strains of *E. coli* (F. J. Trueba, thesis, University of Amsterdam, 1981). A variety of methods applied to analyzing the growth of individual cells, ranging from comparison with theoretical distributions (26, 28, 32; W. J. Voorn, thesis, University of Amsterdam, 1983) to applications of the Collins-Richmond principle (18, 29, 38), appear to agree that elongation of rod-shaped bacteria is exponential. Kubitschek (39), using a cylinder with hemispherical caps as an approximation to cell shape, has shown that in *E. coli* length extension may be exponential, but surface area and volume may increase bilinearly owing to fluctuations in diameter (53). Autoradiographic studies of *E. coli* (13) and *Myxococcus xanthus* (59) have shown that there is an exponential increase in the macromolecular mass of individual cells. The density of *E. coli*, at any particular growth rate, also appears to be essentially constant (25, 31, 57), so that bilinear growth in volume (30) might arise solely from fluctuations in diameter rather than by variation in factors contributing to cell mass, such as the protein content of the cell. There does not appear to be any significant change in diameter with increase of length in *B. subtilis* (2, 53), suggesting that surface area and volume might also increase exponentially. However, cell shape can be only approximately simulated by a cylinder with hemispherical caps (6), so that growth in area or volume might occur by kinetics different to those of increase in length.

To aid interpretation of the results, cell length is shown plotted as a function of time in Fig. 8, from calculations with the Collins-Richmond equation. Again, the results are consistent with exponential growth. The growth rate $V(l)$ calculated by the Collins-Richmond equation suggests that all cells of size l grow at the rate V. Clearly, when the sample is further classified, as reported here, the rate $V(l)$ is an average of the distribution of rates for all cells of size l.

In common with studies of *E. coli* (29) the present results show that length at particular events of the cell cycle is subject to appreciable variation. This feature, in turn, raises two problems: first, how to describe accurately the growth of the "average" cell, and, second, the implication that, were changes in growth rate to occur, the transition point would not occur at a unique size but would be characterized by a defined mean and coefficient of variation. Therefore, application of the Collins-Richmond equation would tend to blur sharp changes in growth rate unless the sample can be subdivided in some way. Even when this approach is used, there can be significant overlap between the three major categories into which cells were placed in the present study (Fig. 6). Thus, mononucleate cells of length >1.0 μm apparently grow at a rate that is different from that of a binucleate cell of the same size. Conversely, cells of different lengths and stages of the cycle may be growing at the same rate. In Fig. 8 the growth of mononucleate, binucleate, and septate cells is shown in relation to time, using the mean size of newborn and separating cells as reference points. For the binucleate cells, the mean size at chromosome segregation (1.21 μm) was placed at 70 min before cell separation, as determined from the theoretical age distribution. Growth is again seen to resemble most closely an exponential pattern; although the classes overlap, the trend is very similar to that determined with the Collins-Richmond equation.

Nucleoid segregation in relation to growth. Our data strongly suggest that extension of the nucleoid is closely paralleled by cell length extension. Only among the septate cells is there deviation from this pattern (Fig. 7), presumably because there is a slight reduction in length of daughter nucleoids immediately after segregation (Fig. 5). Unlike the prediction of the original replicon hypothesis (22), segregation does not therefore appear to occur at termination but proceeds continuously (36, 56). Although nucleoid distance has been measured, the evident coincidence of cell extension and nucleoid migration must presumably reflect the underlying coupling of both processes. It is also clear that the distal poles (g in Fig. 5) show no appreciable growth, in agreement with measurements of pole dimensions (6) and the limited amount of wall turnover detected in older poles (35). The implication of this observation is that the extent of the cylindrical growth "zone" lies between the distal tips of the nucleoids, excluding the contribution of nascent poles, i.e., $a - 2e$ in Fig. 4 and 5 (18). The older poles may also include a portion of the cylindrical wall, because the nucleoids do not always appear to extend to the presumed junction of polar and cylindrical wall (Fig. 4). These distal tips could possibly be equivalent to the "polar sheaths" detected by autoradiography (51) or immunofluorescence (7). Production of minicells without DNA (45) may also occur at this location and perhaps also at the subterminal swellings reported in *dnaB* mutants of *B. subtilis* held at the restrictive temperature (55).

However, the rate calculations, both for nucleoid and length extension, as discussed above, also show that the growth rate of mononucleate cells may in some cases be greater than that of binucleate cells of the same length. This observation poses a number of difficulties in accepting the conclusion that nucleoid extension is truly coupled to length extension. There are several possible causes from which this difficulty in interpretation might arise. The first concerns the stochastic variation in the length at which chromosome segregation occurs; the coefficient of variation was about 13% (Table 1). The second aspect may involve a more subtle modulation in growth pattern concerned with the entry of cells into the septation sequence. The rate of nucleoid extension in septate cells (Fig. 7) does not exactly parallel the rate of length extension. One possibility, therefore, is that the rate of nucleoid and cell extension is greatest at stages preceding and including chromosome segregation but gradually declines when the cells are fully binucleate. As shown in Fig. 5, when the mean values for nucleoid length ($a - 2e$ in Fig. 4) are plotted as a function of mean cell length, the relationship becomes nonlinear among septate classes, showing a pronounced decline. At this stage, that portion of the cylindrical wall (c in Fig. 4) adjacent to the developing poles (e in Fig. 4) is also increasing with cell length. Thus, in spite of contributions to growth from locations c and n, the total rate of nucleoid ($a - 2e$ in Fig. 4) extension is actually decreasing during septation. The possibility therefore exists that growth is maximal in mononucleate and binucleate cells, where nucleoid extension is most evidently coupled to length extension but actually decreases during septation. The

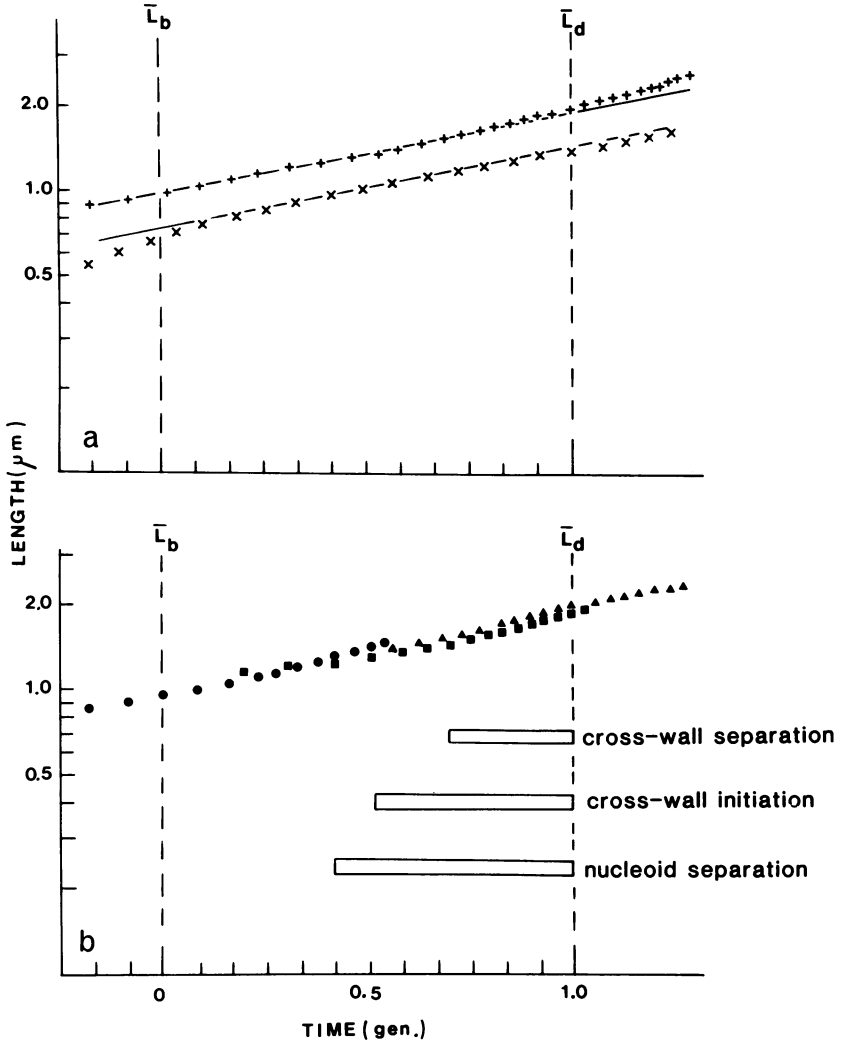

FIG. 8. (a) Relationship of cell length to time determined by the Collins-Richmond equation and data shown in Fig. 6. Length (+) is exponential, as is growth of nucleoid distance (×), i.e., $(a - 2e)$; both lines are parallel. (b) Growth with respect to time of mononucleate (●), binucleate (■), and septate (▲) cells, using the mean length of newborn ($\bar{L}_b$) and separating ($\bar{L}_d$) cells to mark the start and end of the cycle. Events of the cycle indicated include nuclear segregation, cross-wall initiation, and cross-wall separation determined from the theoretical age distribution (see the text).

marked "acceleratedly exponential" pattern of length extension (Fig. 6) would then concern only those organisms larger than the mean size at septation.

Exponential growth kinetics tend to be interpreted in terms of diffuse growth over the cell surface, in contrast to linear growth arising from addition of nascent wall at a constant rate to an annular growth zone (37). More difficult to distinguish is growth from an exponentially increasing series of growth sites or one site operating at an increasing, exponential rate. However, if our results do indeed reveal coordinate growth of surface and nucleoid, then the growth pattern of the nucleoid (Fig. 7) is more easily interpretable as an exponentially increasing number of attachment points of nucleoids to envelope (12, 33, 34, 49). Presumably, therefore, the number of wall biosynthetic sites is increasing in the same manner.

Schlaeppi and Karamata (50) obtained evidence for the cosegregation of wall and DNA in *B. subtilis*. After several generations, old wall apparently segregates into several units, and the number of segregation units may be determined by the frequency of initiation of chromosome replication. In contrast, similar autoradiographic studies of *B. subtilis* by Mobley et al. (35) suggested that, apart from the old poles, no part of the cell surface conserves label and that chase periods exceeding 3 to 3.5 generations may not be reliable because the label is not then incorporated quantitatively. In streptococci, termination of chromosome replication is necessary for completion of division processes such as septation, but initiation of a growth site is not apparently correlated with inauguration of chromosome replication. Instead, a fixed volume of wall is generated per growth site, independent of the doubling time (16).

In conclusion, we envisage that length extension in *B. subtilis* occurs exponentially and that classification of the cells into mononucleate, binucleate, and septate offers a sensitive way in which to test for possible changes of growth rate. At no stage of the cycle is there any conspicuous change in growth rate. The portion of the cell lying between

the distal edges of the nucleoid, but excluding the nascent poles, may represent the cylindrical surface. Growth of this presumed cylindrical site occurs at the same rate as length extension of the cell.

APPENDIX

Here we give an outline of the derivation of the equations used to calculate the growth rate of mononucleate, binucleate, and septate cells. A more complete description will be published elsewhere (Kirkwood and Burdett, in preparation).

Consider a population of cells in exponential growth, maintained in a steady state with specific growth rate k. If the total number of cells at some time $t = 0$ is N_0, the number at time t is N_0e^{kt}. Suppose that the cells can be divided into three distinct subclasses as (i) mononucleate, (ii) binucleate, and (iii) septate, and let the numbers of cells in each class at time $t = 0$ be M_0, B_0, and S_0, respectively, so that $N_0 = M_0 + B_0 + S_0$. Because growth is in a steady state, the corresponding numbers of mononucleate, binucleate, and septate cells at time t will be M_0e^{kt}, B_0e^{kt}, and S_0e^{kt}, respectively. M_0, B_0, and S_0 thus determine the proportions of the total population that belong to each class at any given time.

Let $\lambda^M(l)$, $\lambda^B(l)$, and $\lambda^S(l)$ denote the frequency distributions of cell lengths (l) within the three classes. Then the overall distribution of length in the population is

$$\lambda(l) = \frac{M_0\lambda^M(l) + B_0\lambda^B(l) + S_0\lambda^S(l)}{M_0 + B_0 + S_0} \qquad \text{(A1)}$$

Also, let $\phi(l)$ be the frequency distribution of lengths of dividing cells, $\psi(l)$ be the frequency distribution of lengths of newborn cells, $\theta(l)$ be the frequency distribution of lengths of cells at the time of chromosome segregation (i.e., transfer from class M to class B), and $\chi(l)$ be the frequency distribution of the lengths of cells at the time of cross wall initiation (i.e., transfer from class B to class S).

Following the approach of Collins and Richmond (8, 18), we calculate the growth rates of cells by considering their entry into and exit from the B, M, and S subclasses, subject to the constraint of steady-state growth.

Mononucleate cells. Consider the set of mononucleate cells with lengths in the range (l to ∞) for some length $l > 0$. The number of cells in this set is

$$M_0e^{kt}\int_l^\infty \lambda^M(x)dx$$

and the rate of increase in this number is

$$kM_0e^{kt}\int_l^\infty \lambda^M(x)dx$$

This rate of increase is made up of three terms: the rate at which shorter mononucleate cells grow into the range (l, ∞), the rate at which new cells are born into the range (l, ∞), and the rate at which mononucleate cells transfer into the binucleate class by undergoing chromosome segregation. The first two of these terms are positive, whereas the third is negative. Formally, the equation can be represented as

$$kM_0e^{kt}\int_l^\infty \lambda^M(x)dx = M_0e^{kt}V^M(l)\,\lambda^M(l) + 2kN_0e^{kt}\int_l^\infty \psi(x)dx - r_{MB}M_0e^{kt}\int_l^\infty \theta(x)dx \qquad \text{(A2)}$$

where $V^M(l)$ is the rate of growth (i.e., length extension) of mononucleate cells of length l and r_{MB} is the overall rate at which mononucleate cells become binucleate.

Binucleate cells. Similarly, the rate of increase in the number of binucleate cells can be represented as the combined result of the rate at which shorter binucleate cells grow into the range (l to ∞), the rate at which mononucleate cells become binucleate (now a positive term), and the rate at which binucleate cells transfer into the septate class by initiating the formation of cross wall (negative term). This gives

$$kB_0e^{kt}\int_l^\infty \lambda^B(x)dx = B_0e^{kt}V^B(l)\,\lambda^B(l) + r_{MB}M_0e^{kt}\int_l^\infty \theta(x)dx - r_{BS}B_0e^{kt}\int_l^\infty \chi(x)dx \qquad \text{(A3)}$$

where $V^B(l)$ is the rate of growth of binucleate cells of length l, and r_{BS} is the overall rate at which binucleate cells become septate.

Septate cells. For the septate cells the rate of increase in the number of cells in the length range (l to ∞) is made up of the rate at which shorter septate cells grow into the range (l to ∞), the rate at which binucleate cells become septate (now a positive term), and the rate at which septate cells undergo division (negative term). This gives

$$kS_0e^{kt}\int_l^\infty \lambda^S(x)dx = S_0e^{kt}V^S(l)\,\lambda^S(l) + r_{BS}B_0e^{kt}\int_l^\infty \chi(x)dx - kN_0e^{kt}\int_l^\infty \phi(x)dx \qquad \text{(A4)}$$

where $V^S(l)$ is the rate of growth of septate cells of length l.

The rate constants r_{MB} and r_{BS} can be determined by taking the value of l to be 0 in equations A2 and A4. Since the integrals from 0 to ∞ of each of the frequency distributions are 1, and since $\lambda^M(0) = \lambda^S(0) = 0$ (as there can be no cells of 0 length), the equations reduce to $kM_0e^{kt} = 2kN_0e^{kt} - r_{MB}M_0e^{kt}$ and $kS_0e^{kt} = r_{BS}B_0e^{kt} - kN_0e^{kt}$. Rearranging these equations and cancelling through by e^{kt} gives $r_{MB} = k(N_0 + B_0 + S_0)/M_0$ and $r_{BS} = k(N_0 + S_0)/S_0$.

The rates of growth $V^M(l)$, $V^B(l)$, and $V^S(l)$ of mononucleate, binucleate, and septate cells of length l can then be determined from equations (A2), (A3), and (A4) as

$$V(l) = \left[kM_0\int_l^\infty \lambda^M(x)dx - 2kN_0\int_l^\infty \psi(x)dx + r_{MB}M_0\int_l^\infty \theta(x)dx\right] \Big/ M_0\lambda^M(l)$$

$$V(l) = \left[kB_0\int_l^\infty \lambda^B(x)dx - r_{MB}M_0\int_l^\infty \theta(x)dx + r_{BS}B_0\int_l^\infty \chi(x)dx\right] \Big/ B_0\lambda^B(l)$$

$$V(l) = \left[kS_0\int_l^\infty \lambda^S(x)dx - r_{BS}B_0\int_l^\infty \chi(x)dx + kN_0\int_l^\infty \phi(x)dx\right] \Big/ S_0\lambda^S(l)$$

where r_{MB} and r_{BS} are given as above and the frequency distributions ϕ, ψ, θ, χ, λ^M, λ^B, and λ^S are estimated from experimental data as follows.

Estimation of frequency distributions. As described in the text, cells were classified from the electron micrographs into seven categories: mononucleate (M), chromosome segregation (CS), binucleate 1 (B1), binucleate 2, (B2), cross-wall initiation (CWI), midseparating (MS), and fully separating cells (FS). The length distributions within these categories were compiled as histograms. The problem is to use these data to determine the frequency distributions ϕ, ψ, θ, χ, λ^M, λ^B, and λ^S.

In the theory described above, the transitions between the mononucleate, binucleate, and septate stages of the cell cycle and the moment of cell division are assumed to be sharply defined. Thus, at any given moment the number of cells in the population actually at the transition points should be effectively zero. In practice, however, there will be many cells so close to the transition points that it cannot be decided by observation on which side they lie. For the purposes of computing the cell growth rates it is necessary that all cells should be allocated to one or another of the length distributions λ^M, λ^B, and λ^S, and at the same time the cells near to the transition points should be used to estimate ϕ, ψ, θ, and χ.

The procedures adopted for each of the seven cell categories scored experimentally were as follows. First, for the cells which were clearly between transition points, i.e., categories M, B1, B2, and MS, the cells were allocated directly to the appropriate length distribution λ^M, λ^B, or λ^S. For the cells apparently on the point of cell division (category FS), it was assumed that although this category comprised cells not exactly at the point of division, but only very near to it, negligible growth would take place before cell division was completed. Therefore, the frequency distribution of whole cell lengths was taken as the estimate for ϕ, and the frequency distribution of daughter cell lengths was taken as the estimate for ψ. By similar reasoning each of the category FS cells was regarded as being so close to the point of division that it might equally be regarded as a single septate cell or as two mononucleate cells. Thus, one half of the histogram of category FS whole-cell lengths was allocated to forming the length distribution λ^S, and one half of the histogram of category FS daughter cell lengths was allocated to forming the length distribution λ^M (by one half of the histogram is meant one half of the number of cells in each length group).

The remaining two categories of cells (CS and CI) required special consideration, since the transition points between the mononucleate and binucleate classes and between the binucleate and septate classes are less easily defined in terms of features which can be identified precisely in the electron micrographs. It was likely, therefore, that the cells scored in categories CS and CI would include some cells which either had grown a little since passing the transition point or would grow before reaching it. The frequency distributions of the CS and CI cells were thus taken as the outside estimates for θ and χ. As described in the text, narrower estimates for θ and χ were also considered. For these narrower estimates, it was assumed that there was an equal likelihood of including cells which were too long and too short in the categories CS and CI, and so the reduced width estimates for θ and χ were obtained by retaining the same mean but reducing the standard deviation of the length distributions of the CS and CI cells. This was done by using a log normal distribution for θ and χ, since the length distributions of the CS and CI cells were positively skewed and showed a good fit to this model.

Finally, as with the FS cells it was necessary to allocate the CS and CI cells to the λ^M, λ^B, and λ^S distributions. When the frequency distributions of the CS and CI cells were used directly to estimate θ and χ, this was done by allocating half of the CS histogram to each of λ^M and λ^B and half of the CI histogram to each of λ^B and λ^S. When a narrower frequency distribution was used, equivalent to assuming that the shorter CS or CI cells were likely to be before the transition point and the longer CS or CI cells were likely to be after the transition point, the shorter CS and CI cells were preferentially allocated to λ^M and λ^B, and the longer CS and CI cells were preferentially allocated to λ^B and λ^S, respectively. The method used to carry out this allocation will be described in detail elsewhere (Kirkwood and Burdett, in preparation); essentially, the allocation is determined by using the cumulative frequency for the assumed θ or χ distribution so that, when the likelihood of a cell having reached the transition point is small, it is correspondingly allocated with higher probability to the earlier class, and conversely.

Average cell growth. The method we used to calculate the growth rates of mononucleate, binucleate, and septate cells is an extension of the standard Collins-Richmond (8) analysis. Its relationship to the standard method can be seen when equations A2, A3, and A4 are added together. This gives

$$kM_0e^{kt}\int_l^\infty \lambda^M(x)dx + kB_0e^{kt}\int_l^\infty \lambda^B(x)dx +$$

$$kS_0e^{kt}\int_l^\infty \lambda^S(x)dx = M_0e^{kt}V^M(l)\lambda^M(l) + B_0e^{kt}V^B(l)\lambda^B(l) +$$

$$S_0e^{kt}V^S(l)\lambda^S(l) + 2kN_0e^{kt}\int_l^\infty \psi(x)dx - kN_0e^{kt}\int_l^\infty \phi(x)dx$$

The left-hand side of this equation, from equation A1, is simply

$$kN_0e^{kt}\int_l^\infty \lambda(x)dx$$

and cancelling through by e^{kt} and noting that the standard Collins and Richmond expression for the growth rate of cells of length l is

$$V(l) = \left[k\int_l^\infty \lambda(x)dx - 2k\int_l^\infty \psi(x)dx + k\int_l^\infty \phi(x)dx\right] \Big/ \lambda(l)$$

we have $V(l) = [M_0V^M(l) + B_0V^B(l) + S_0V^S(l)]/N_0$. In other words, the growth rate obtained from the standard Collins-Richmond analysis is simply the average growth rate of the mononucleate, binucleate, and septate cells weighted according to the numbers of cells in each class.

LITERATURE CITED

1. **Archibald, A. R., and H. E. Coapes.** 1976. Bacteriophage SP50 as a marker for cell wall growth in *Bacillus subtilis*. J. Bacteriol. **125**:1195–1206.
2. **Burdett, I. D. J.** 1979. Electron microscope study of the rod-to-coccus shape change in a temperature-sensitive Rod$^-$ mutant of *Bacillus subtilis*. J. Bacteriol. **137**:1395–1405.
3. **Burdett, I. D. J.** 1980. Quantitative studies of rod-coccus morphogenesis in a temperature-sensitive Rod$^-$ mutant of *Bacillus subtilis*. J. Gen. Microbiol. **121**:93–103.
4. **Burdett, I. D. J., and M. L. Higgins.** 1978. Study of pole assembly in *Bacillus subtilis* by computer reconstruction of septal growth zones seen in central, longitudinal thin sections of cells. J. Bacteriol. **133**:959–971.
5. **Burdett, I. D. J., and T. B. L. Kirkwood.** 1983. How does a bacterium grow during its cell cycle? J. Theor. Biol. **103**:11–20.
6. **Burdett, I. D. J., and A. L. Koch.** 1984. Shape of nascent and completed poles of *Bacillus subtilis*. J. Gen. Microbiol. **130**:1711–1722.
7. **Chung, K. L., R. Z. Hawirko, and P. K. Isaac.** 1964. Cell wall replication. I. Cell wall growth of *Bacillus cereus* and *Bacillus megaterium*. Can. J. Microbiol. **10**:43–48.
8. **Collins, J. F., and M. H. Richmond.** 1962. Rate of growth of *Bacillus cereus* between divisions. J. Gen. Microbiol. **28**:15–33.
9. **Cook, J. R., and T. W. James.** 1964. Age distribution of cells in logarithmically growing cell populations, p. 485–495. *In* E. Zeuthen (ed.), Synchrony in cell division and growth. John Wiley & Sons, Inc., New York.
10. **Cooper, S., and C. E. Helmstetter.** 1968. Chromosome replication and the division cycle of *Escherichia coli*. Br. J. Mol. Biol. **31**:519–540.
11. **De Chastellier, C., R. Hellio, and A. Ryter.** 1975. Study of cell wall growth in *Bacillus megaterium* by high-resolution autoradiography. J. Bacteriol. **123**:1184–1196.
12. **Doyle, R. J., A. L. Koch, and P. H. B. Carstens.** 1983. Cell wall-DNA association in *Bacillus subtilis*. J. Bacteriol. **153**:1521–1527.
13. **Ecker, R., and G. Kokaisl.** 1969. Synthesis of protein,

ribonucleic acids, and ribosomes by individual bacterial cells in balanced growth. J. Bacteriol. **98**:1219–1226.
14. **Ephrati-Elizur, E., and S. Borenstein.** 1971. Velocity of chromosome replication in thymine-requiring and independent strains of *Bacillus subtilis*. J. Bacteriol. **106**:58–64.
15. **Errington, F. P., E. O. Powell, and N. Thompson.** 1965. Growth characteristics of some gram-negative bacteria. J. Gen. Microbiol. **39**:109–123.
16. **Gibson, C. W., L. Daneo-Moore, and M. L. Higgins.** 1983. Initiation of wall assembly sites in *Streptococcus faecium*. J. Bacteriol. **154**:573–579.
17. **Hariharan, I. K., R. Czolij, and R. G. Wake.** 1982. Conformation and segregation of nucleoids accompanying cell length extension after completion of a single round of DNA replication in germinated and outgrowing *Bacillus subtilis* spores. J. Bacteriol. **150**:861–869.
18. **Harvey, R. J., A. G. Marr, and P. R. Painter.** 1967. Kinetics of growth of individual cells of *Escherichia coli* and *Azotobacter agilis*. J. Bacteriol. **93**:605–617.
19. **Higgins, M. L., and G. D. Shockman.** 1976. Study of a cycle of cell wall assembly in *Streptococcus faecalis* by three-dimensional reconstructions of thin sections of cells. J. Bacteriol. **127**:1346–1358.
20. **Highton, P. J.** 1970. An electron microscope study of mesosomes in *Bacillus subtilis*. J. Ultrastruct. Res. **31**:260–271.
21. **Hughes, R. C., and E. Stokes.** 1971. Cell wall growth in *Bacillus licheniformis* followed by immunofluorescence with mucopeptide-specific antiserum. J. Bacteriol. **106**:694–696.
22. **Jacob, F., S. Brenner, and F. Cuzin.** 1963. On the regulation of DNA replication in bacteria. Cold Spring Harbor Symp. Quant. Biol. **28**:329–348.
23. **Kellenberger, E., A. Ryter, and J. Sechaud.** 1958. Electron microscope study of DNA-containing plasms. II. Vegetative and mature phage DNA as compared with normal bacterial nucleoids in different physiological states. J. Biophys. Biochem. Cytol. **4**:671–676.
24. **Koch, A. L.** 1983. The surface stress theory of microbial morphogenesis. Adv. Microb. Physiol. **24**:301–367.
25. **Koch, A. L., and G. Blumberg.** 1976. Distribution of bacteria in the velocity gradient centrifuge. Biophys. J. **16**:389–405.
26. **Koch, A. L., and M. L. Higgins.** 1982. Cell cycle dynamics inferred from the static properties of cells in balanced growth. J. Gen. Microbiol. **128**:2877–2892.
27. **Koch, A. L., H. L. Y. Mobley, R. J. Doyle, and U. N. Streips.** 1981. The coupling of wall growth and chromosome replication in gram-positive rods. FEBS Lett. **12**:201–208.
28. **Koch, A. L., and M. Schaecter.** 1962. A model for statistics of the cell division process. J. Gen. Microbiol. **29**:435–454.
29. **Koppes, L. J. H., C. L. Woldringh, and N. Nanninga.** 1978. Size variations and correlation of different cell cycle events in slow-growing *Escherichia coli*. J. Bacteriol. **134**:423–433.
30. **Kubitschek, H. E.** 1981. Bilinear cell growth of *Escherichia coli*. J. Bacteriol. **148**:730–733.
31. **Kubitschek, H. E., W. A. Baldwin, and R. Graetzer.** 1983. Buoyant density constancy during the cell cycle of *Escherichia coli*. J. Bacteriol. **155**:1027–1032.
32. **Kubitschek, H. E., and C. L. Woldringh.** 1983. Cell elongation and division probability during the *Escherichia coli* growth cycle. J. Bacteriol. **153**:1379–1387.
33. **Kusano, T., D. Steinmetz, W. G. Hendrickson, J. Murchie, M. King, A. Benson, and M. Schaecter.** 1984. Direct evidence for specific binding of the replicative origin of the *Escherichia coli* chromosome to the membrane. J. Bacteriol. **158**:313–316.
34. **Leibowitz, R. J., and M. Schaecter.** 1975. The attachment of the bacterial chromosome to the cell membrane. Int. Rev. Cytol. **41**:1–28.
35. **Mobley, H. L. T., A. L. Koch, R. J. Doyle, and U. N. Streips.** 1984. Insertion and fate of the cell wall in *Bacillus subtilis*. J. Bacteriol. **158**:169–179.
36. **Nanninga, N., L. J. H. Koppes, and F. C. de Vries Tijssen.** 1979. The cell cycle of *Bacillus subtilis* as studied by electron microscopy. Arch. Microbiol. **123**:173–181.
37. **Nanninga, N., and C. L. Woldringh.** 1985. Cell growth, genome duplication and cell division, p. 259–318. *In* N. Nanninga (ed.), Molecular cytology of *Escherichia coli*. Academic Press, Inc., New York.
38. **Nanninga, N., C. L. Woldringh, and L. J. H. Koppes.** 1982. Growth and division of *Escherichia coli*, p. 225–270. *In* C. Nicolini (ed.), Cell growth. Plenum Publishing Corp., New York.
39. **Nermut, M. V.** 1982. The "cell monolayer technique" in membrane research. Eur. J. Cell Biol. **28**:160–172.
40. **Pierucci, O.** 1978. Dimensions of *Escherichia coli* at various growth rates: model for envelope growth. J. Bacteriol. **135**: 559–574.
41. **Pooley, H. M.** 1976. Turnover and spreading of old wall during surface growth of *Bacillus subtilis*. J. Bacteriol. **125**:1127–1138.
42. **Pooley, H. M.** 1976. Layered distribution, according to age, within the cell wall of *Bacillus subtilis*. J. Bacteriol. **125**: 1139–1147.
43. **Previc, E. P.** 1970. Biochemical determination of bacterial morphology and the geometry of cell division. J. Theor. Biol. **27**:471–497.
44. **Pritchard, R. H.** 1974. On the growth and form of a bacterial cell. Philos. Trans. R. Soc. London B **267**:303–336.
45. **Reeve, J. N., N. H. Mendelson, S. J. Coyne, L. L. Hallock, and R. M. Cole.** 1973. Minicells of *Bacillus subtilis*. J. Bacteriol. **114**:860–873.
46. **Sargent, M. G.** 1975. Control of membrane protein synthesis in *Bacillus subtilis*. Biochim. Biophys. Acta **406**:564–574.
47. **Sargent, M. G.** 1975. Control of cell length in *Bacillus subtilis*. J. Bacteriol. **123**:7–19.
48. **Sargent, M. G.** 1979. Surface extension and the cell cycle in prokaryotes. Adv. Microb. Physiol. **18**:105–176.
49. **Sargent, M. G., M. F. Bennett, and I. D. J. Burdett.** 1983. Identification of specific restriction fragments associated with a membrane subparticle from *Bacillus subtilis*. J. Bacteriol. **154**:1389–1396.
50. **Schlaeppi, J. M., and D. Karamata.** 1982. Cosegregation of cell wall and DNA in *Bacillus subtilis*. J. Bacteriol. **152**:1231–1240.
51. **Schlaeppi, J. M., H. M. Pooley, and D. Karamata.** 1982. Identification of cell wall subunits in *Bacillus subtilis* and analysis of their segregation during growth. J. Bacteriol. **149**:329–337.
52. **Siegel, S.** 1956. Nonparametric statistics for the behavioural sciences. McGraw-Hill Kogakusha, Ltd., Tokyo.
53. **Trueba, F. J., and C. L. Woldringh.** 1980. Changes in cell diameter during the division cycle of *Escherichia coli*. J. Bacteriol. **150**:1048–1055.
54. **Valkenburg, J. A. C., C. L. Woldringh, G. J. Brakenhoff, H. T. M. Van der Voort, and N. Nanninga.** 1985. Confocal scanning light microscopy of the *Escherichia coli* nucleoid: comparison with phase-contrast and electron microscope images. J. Bacteriol. **161**:478–483.
55. **Viret, J.-F., H. J. Rogers, and D. Karamata.** 1985. Morphological and cell wall alterations in thermosensitive *dna* mutants of *Bacillus subtilis*. Ann. Inst. Pasteur Microbiol. **136**:119–129.
56. **Woldringh, C. L.** 1976. Morphological analysis of nuclear separation and cell division during the life cycle of *Escherichia coli*. J. Bacteriol. **125**:248–257.
57. **Woldringh, C. L., J. S. Binnerts, and A. Mans.** 1981. Variation in *Escherichia coli* buoyant density measured in Percoll gradients. J. Bacteriol. **148**:58–63.
58. **Woldringh, C. L., M. A. de Jong, W. Van den Berg, and L. Koppes.** 1977. Morphological analysis of the division cycle of two *Escherichia coli* substrains during slow growth. J. Bacteriol. **131**:270–279.
59. **Zusman, D., P. Gottlieb, and E. Rosenberg.** 1971. Division cycle of *Myxococcus xanthus*. III. Kinetics of cell growth and protein synthesis. J. Bacteriol. **105**:811–819.